MAGNETIC RESONANCE IN MEDICINE 19, 233–239 (1991)

Diffusion Imaging Using Stimulated Echoes*

KLAUS-DIETMAR MERBOLDT, WOLFGANG HÄNICKE, AND JENS FRAHM

Max-Planck-Institut für biophysikalische Chemie, Postfach 2841, D-3400 Göttingen, Federal Republic of Germany

Received February 1, 1991

The application of stimulated echo acquisition mode (STEAM) sequences for NMR imaging of diffusion is especially suited for spins with $T_1 \gg T_2$ as, e.g., encountered in proton NMR studies of biological systems. Molecular self-diffusion coefficients may be calculated from a set of diffusion-weighted images acquired with different gradient strengths. A variation of the diffusion time allows the determination of restricted and/or anisotropic diffusion in cellular systems ranging from plants to humans. Problems associated with the presence of unavoidable macroscopic motions *in vivo* are demonstrated in diffusion studies of human brain. Motion ghosting in diffusion-weighted images may be overcome by means of a high-speed STEAM sequence yielding single-shot images within subsecond acquisition times.

The molecular self-diffusion coefficient reflects the mobility of molecules in their microenvironment and, therefore, contains important information about the microscopic structural and dynamic properties of the system under investigation. The use of stimulated echoes (*1*) for NMR diffusion measurements without spatial resolution was first described by Stejskal and Tanner (*2, 3*). For NMR imaging of diffusion, stimulated echo acquisition mode (STEAM) sequences (*4, 5*) frequency- and phase-encoding gradients as shown in Fig. 1a are added. Cross-sectional images require the application of a slice selection gradient in conjunction with at least one frequency-selective 90° rf pulse. Diffusion weighting is accomplished by a pair of balanced gradients (dotted lines) that may be switched simultaneously in two or three directions to increase the effective diffusion weighting or separately in each direction to investigate anisotropic diffusion.

Figure 1b shows a high-speed sequence for STEAM diffusion imaging that is intended to overcome motion problems. For single-shot imaging the final 90° rf pulse is replaced by a series of low flip angle pulses. The respective STE signals are differently phase-encoded so that measuring times of fractions of a second are achieved when using acquisition matrices of 32–64 × 128 pixels. In contrast to the conventional STEAM sequence in Fig. 1a, the middle interval and, thus, also the diffusion time of the high-speed STEAM sequence increase with the number of phase-encoding steps or rf pulse repetitions. However, as long as the total acquisition time remains shorter than the mean diffusion time defined by the time between the first TE/2 interval and the

* Presented at SMRM Workshop on Future Directions in MRI of Diffusion and Microcirculation, Bethesda, MD, June 7 and 8, 1990.

0740-3194/91 $3.00

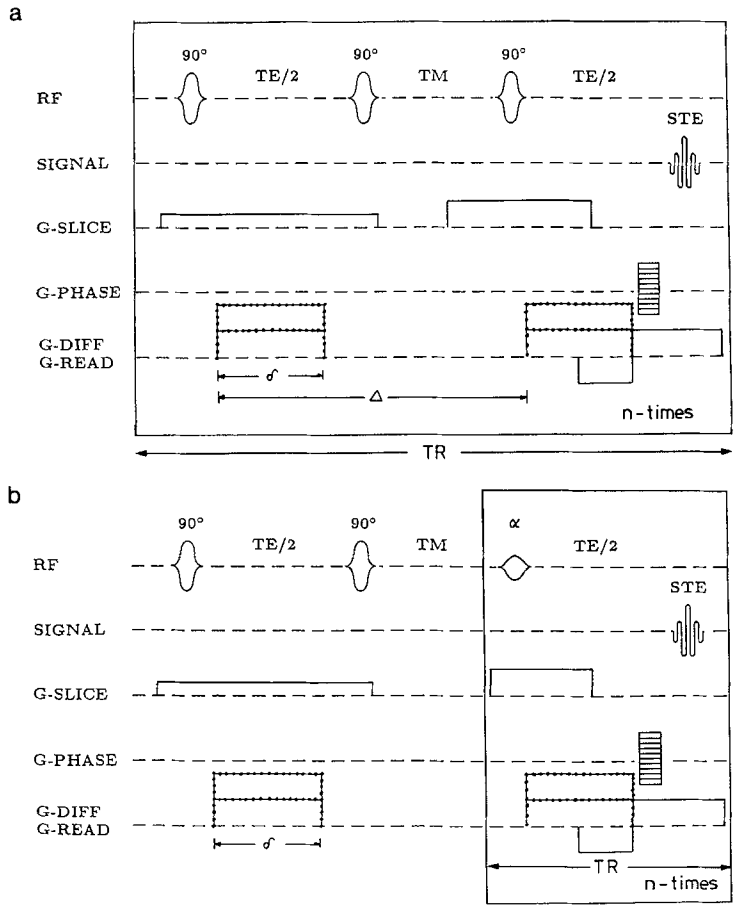

FIG. 1. Schematic rf pulse and gradient sequences for NMR imaging of diffusion using stimulated echoes. (a) Conventional stimulated echo acquisition mode (STEAM) sequence modified for diffusion weighting by the incorporation of a pair of balanced diffusion gradients (G-Diff, dotted line) of duration δ and separation Δ (diffusion time). (b) High-speed version of the diffusion-weighted STEAM sequence where the final 90° rf pulse of sequence (a) is replaced by a series of low flip angle pulses. Diffusion gradients may be applied in one, two, or all three gradient axes.

repetition interval with the zero phase-encoded STE signal, phantom studies show a good agreement with diffusion coefficients determined by other NMR techniques. Details of the high-speed STEAM sequence are described elsewhere (*6–8*). Other modifications of the basic STEAM sequence restrict the imaging plane to a column or even to a "point" for spectroscopic examinations (*9*). Applications to phosphorus NMR spectroscopy have been reported by others (*10*).

The two-dimensional spatial distribution of the self-diffusion coefficient may be represented in a cross-sectional diffusion map. Such data may be calculated from a set of diffusion-weighted images acquired with different gradients. For this purpose the image intensities I measured as a function of gradient strength g are fitted to (*3*)

$$\ln I = D\gamma^2 g^2 \delta^2 (\Delta - \delta/3)$$

on a pixel by pixel basis with γ, δ, and Δ the magnetogyric ratio, the duration, and the separation (diffusion time) of the diffusion gradient pulses. In cases where the free diffusion of molecules is hindered by boundaries, e.g., in cells, the *observed* diffusion coefficient becomes dependent on the diffusion time Δ (*11*).

Imaging studies of restricted diffusion in plants were performed with the use of a 2.35-T 40-cm-bore magnet and a gradient system with a maximum strength of 16 mT m^{-1} (Bruker Medspec). Diffusion measurements on normal human volunteers were carried out on a 2.0-T whole-body NMR system (Siemens Magnetom) equipped with 10 mT m^{-1} gradients. Informed consent was obtained prior to the investigations.

RESULTS AND DISCUSSION

The feasibility and accuracy of diffusion imaging using conventional as well as high-speed STEAM NMR imaging sequences were confirmed in studies of solvents, solvent mixtures, and microemulsions. The various solutions covered a range of self-diffusion coefficients from 0.3 to 2.2 $\times$ 10^{-5} cm^2 s^{-1}. Selected applications to biological systems are described in subsequent sections.

Restricted Diffusion in Plants

NMR imaging of restricted diffusion was investigated in an onion (*12*) using the conventional STEAM sequence described in Fig. 1a. Multiple series of diffusion-weighted images were acquired with gradient strengths of 3.0, 6.0, 8.6, 9.9, and 11.5 mT m^{-1} (δ = 17 ms) and diffusion times ranging from 220 to 1520 ms, respectively. The corresponding attenuation factors $b = \gamma^2 g^2 \delta^2 (\Delta - \delta/3)$ varied from 41 to 4157 s mm^{-1}. Figures 2a–2d show calculated diffusion maps of the onion for diffusion times of 220(a), 420(b), 620(c) and 1020 ms(d). The brightest intensities correspond to a diffusion coefficient of about 1.0 $\times$ 10^{-5} cm^2 s^{-1}. Obviously, the observed values decrease with increasing diffusion time indicating that the diffusion of the intracellular water becomes restricted. This finding is more pronounced in the small cells of the onion core than in the larger outer shells.

The behavior of the D value as a function of diffusion time, i.e., the duration of the TM interval, is depicted in Fig. 2e for the inner core (triangle) and an outer shell (squares) of the onion. The approximate cell radius and the limiting diffusion coefficient in the absence of restriction were obtained by fitting the data to a theoretical description for particles diffusing in a spherical volume with impermeable boundaries (*13*). The evaluated cell radii of 40 μm (core) and 60 μm (shell) are in good agreement with microscopic determinations of the cell sizes of the investigated onion.

Human Studies

The application of diffusion imaging to animals and humans is compromised by the unavoidable presence of macroscopic motions, e.g., CSF-induced pulsations of the brain. While related ghosting artifacts may be reduced by means of EKG-synchronization, the applications of strong diffusion gradients amplifies even small motion-induced phase errors in the NMR signals. The effect is demonstrated in Fig. 3 where

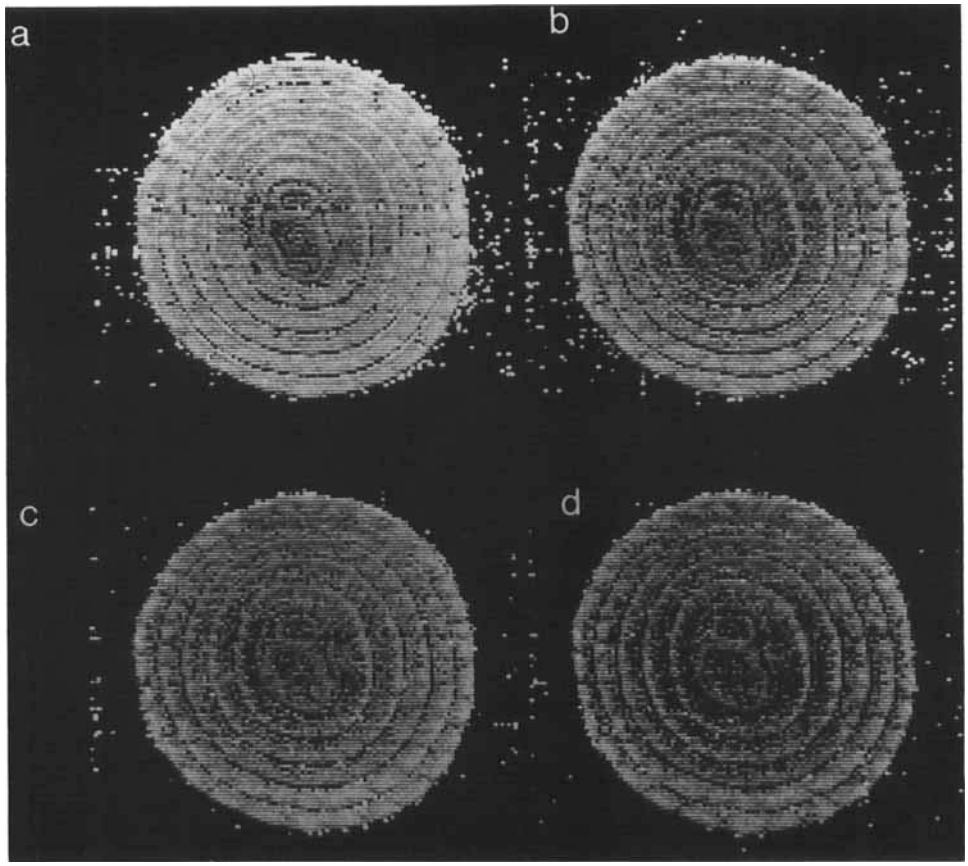

FIG. 2. (a–d) Diffusion maps of an onion calculated from four different sets of diffusion-weighted images acquired with diffusion times of 220 (a), 420 (b), 620 (c), and 1020 ms (d), respectively. The attenuation factors b varied from 41 to 4157 s mm^{-2}. The brightest image intensities correspond to diffusion coefficients of about 1.0×10^{-5} cm^2 s^{-1}. (e) Diffusion coefficients within selected regions-of-interest (3×3 pixels) as a function of diffusion time. The data for an outer shell (squares) and the inner core (triangle) of the onion were fitted to a theory for a particle diffusing in a spherical volume with impermeable boundaries (solid lines). The fit yields cell radii of 40 μm (core) and 60 μm (shell) in agreement with light microscopy. Reprinted, by permission of the publisher, from Ref. (*12*).

a regular fast scan FLASH image of the brain of a normal human volunteer (a) is compared to conventional diffusion-weighted STEAM images without (b) and with EKG-triggering (c). Although the visibility of residual *incoherent* artifacts can be further reduced by signal averaging, the corresponding signal losses in brain tissue must not be misinterpreted as diffusion attenuation (*14*). Consequently, quantitative evaluations of diffusion coefficients *in vivo* or even attempts to separate the relative contributions from diffusion and perfusion must remain ambiguous in the presence of motion.

Figure 3d shows a diffusion-weighted single-shot image acquired with the high-speed STEAM sequence described in Fig. 1b. Although the high-speed approach trades off image resolution for speed, the significant advantage of diffusion-weighted subsecond

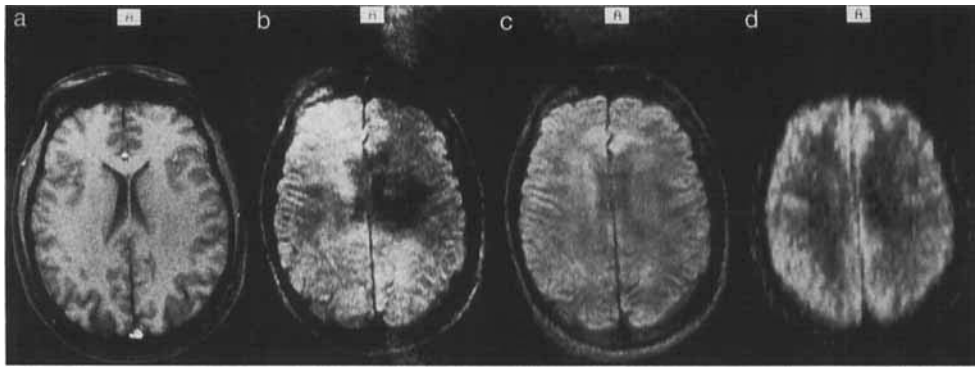

FIG. 3. The influence of brain pulsations in NMR imaging of diffusion as shown in 84-MHz (2.0-T) images of the brain of a normal volunteer. (a) Regular T_1-weighted FLASH image (TR = 100 ms, TE = 6 ms, $\alpha = 70°$); (b) diffusion-weighted STEAM image according to the sequence shown in Fig. 1a ($\delta = 23$ ms, $\Delta = 400$ ms, and G-Diff = 6.53 mT m^{-1} yielding an attenuation factor $b = 646$ s mm^{-2}); (c) diffusion-weighted STEAM image using EKG-triggering (300 ms delay to R wave, other parameters as in (b)); and (d) diffusion-weighted single-shot STEAM image according to the sequence shown in Fig. 1b with a total image acquisition time of 576 ms (48 × 128 data matrix, $\delta = 8.9$ ms, mean $\Delta = 1000$ ms, and G-Diff = 11.3 mT m^{-1} yielding a factor $b = 726$ s mm^{-2}). While high-speed acquisitions are able to *eliminate* motion-induced ghosting artifacts, EKG triggering of conventional STEAM images is only capable of *reducing* their intensities.

imaging is the *elimination* rather than a *reduction* of motion ghosting in particular when EKG-triggering allows the entire image acquisition to be completed within the diastolic phase of a single cardiac cycle. Thus, signal averaging of images from separate heartbeats will not compromise the diffusion attenuation. Accordingly, Figs. 4a–4c and 4e–4g depict diffusion-weighted high-speed STEAM images of the human brain that represent the average of eight accumulations. The diffusion gradient strengths increase from left to right in conjunction with a mean diffusion time of $\Delta = 1000$ ms. Therefore, the relatively short T_1 relaxation time of white matter leads to low image intensities in contrast to its bright appearance relative to gray matter in T_1-weighted FLASH images (Fig. 3a). The images in Figs. 4d and 4h represent diffusion maps that were calculated from a set of four differently diffusion-weighted images. Typical values for diffusion coefficients in white and gray matter range from 0.3 to 1.0 × 10^{-5} cm^2 s^{-1}. Studies of anisotropic diffusion in human brain using a high-speed STEAM imaging sequence are reported elsewhere (*8*).

CONCLUSIONS

Stimulated echo sequences are superior to spin-echo sequences for NMR imaging of diffusion as long as $T_1 \gg T_2$. Moreover, restricted diffusion may be investigated without T_2 signal losses by varying the middle interval of the STEAM sequence. In living subjects diffusion imaging is compromised by ghosting artifacts that are due to unavoidable motions in the presence of the strong diffusion gradients. This also holds for the use of EKG-synchronization. The most promising approach to eliminate motion-related phase inconsistencies from one heartbeat to the next arises from single-

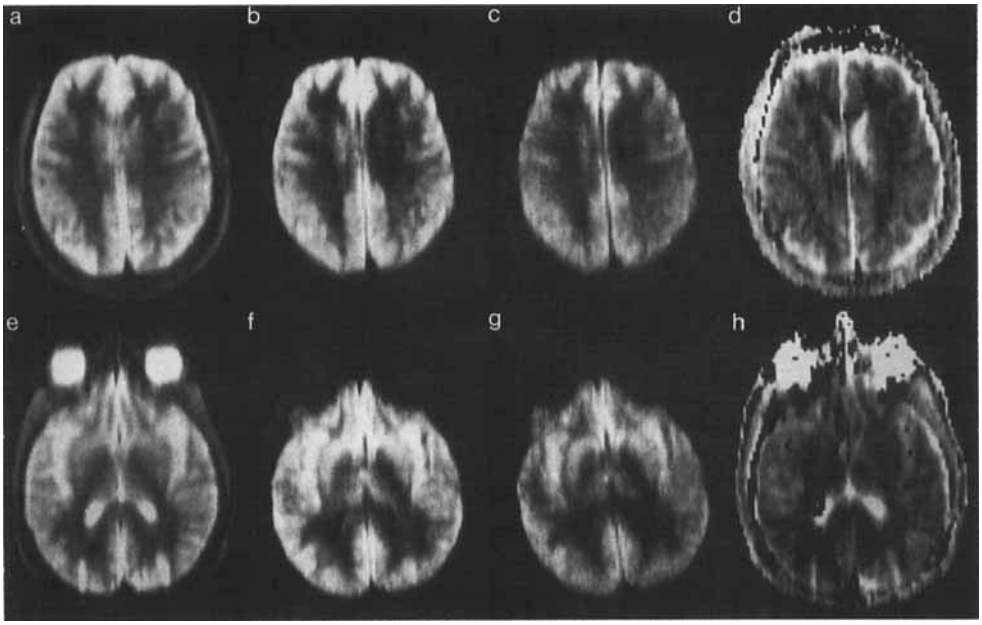

FIG. 4. (a–d) Eighty-four megahertz (2.0-T) diffusion-weighted high-speed STEAM images of the brain of a normal volunteer. (a–c) Three diffusion-weighted images out of a series of four images with gradient strengths of 1.42 mT m^{-1} (a), 9.2 mT m^{-1} (b), and 11.3 mT m^{-1} (c), respectively. Using δ = 8.9 ms and Δ = 1000 ms the corresponding attenuation factors b yield 10, 484, and 726 s mm^{-2}. The images were acquired using a 300-ms delay to the R wave with diffusion gradients in both the frequency-encoding and slice selection directions. They represent the average of eight accumulations from different heartbeats with a minimum of 10 s apart. Image (d) is a calculated diffusion map with the brightest intensities corresponding to diffusion coefficients of $\geq 2.0 \times 10^{-5}$ cm^2 s^{-1}. The same parameters apply to the diffusion-weighted images shown in (e–g) and the related calculated diffusion map in (h).

shot subsecond imaging preferably gated to end diastole. Such studies may be performed using diffusion-weighted high-speed STEAM sequences in close analogy to recent applications of diffusion-weighted echo-planar imaging (*15*).

ACKNOWLEDGMENT

Financial support by the Bundesminister für Forschung und Technologie (BMFT) of the Federal Republic of Germany (Grant 01 VF 8606/6) is gratefully acknowledged.

REFERENCES

1. E. L. HAHN, *Phys. Rev.* **80,** 580 (1950).
2. E. O. STEJSKAL AND J. E. TANNER, *J. Chem. Phys.* **42,** 288 (1964).
3. J. E. TANNER, *J. Chem. Phys.* **52,** 2523 (1970).
4. J. FRAHM, W. HÄNICKE, K.-D. MERBOLDT, AND A. HAASE, *J. Magn. Reson.* **64,** 81 (1985).
5. K.-D. MERBOLDT, W. HÄNICKE, AND J. FRAHM, *J. Magn. Reson.* **64,** 479 (1985).
6. J. FRAHM, A. HAASE, D. MATTHAEI, K.-D. MERBOLDT, AND W. HÄNICKE, *J. Magn. Reson.* **65,** 130 (1985).
7. J. FRAHM, W. HÄNICKE, H. BRUHN, M. L. GYNGELL, AND K.-D. MERBOLDT, *Magn. Reson. Med.*, in press.

8. K.-D. MERBOLDT, W. HÄNICKE, H. BRUHN, M. L. GYNGELL, AND J. FRAHM, *Magn. Reson. Med.*, in press.
9. J. FRAHM, K.-D. MERBOLDT, AND W. HÄNICKE, *J. Magn. Reson.* **72,** 502 (1987).
10. C. T. W. MOONEN, P. C. M. VAN ZIJL, D. LEBIHAN, AND D. DESPRES, *Magn. Reson. Med.* **13,** 467 (1990).
11. R. C. WAYNE AND R. M. COTTS, *Phys. Rev.* **151,** 264 (1966).
12. K.-D. MERBOLDT, W. HÄNICKE, AND J. FRAHM, *Ber. Bunsenges. Phys. Chem.* **91,** 1124 (1987).
13. J. S. MURDAY AND R. M. COTTS, *J. Chem. Phys.* **48,** 4938 (1968).
14. K.-D. MERBOLDT, W. HÄNICKE, M. L. GYNGELL, J. FRAHM, AND H. BRUHN, *Magn. Reson. Med.* **12,** 198 (1989).
15. R. TURNER AND D. LEBIHAN, *J. Magn. Reson.* **86,** 445 (1990).